Journal of Materials Science and Chemical Engineering, 2016, 4, 8-14
Published Online July 2016 in SciRes. http://www.scirp.org/journal/msce
http://dx.doi.org/10.4236/msce.2016.47002

Microstructure of Plasma Sprayed Al_2O_3-3wt%TiO_2 Coating Using Freeze Granulated Powder

Yiming Yao[1*], Ola Lyckfeldt[2], Aurélien Tricoire[3], Dennis Lundström[3], Uta Klement[1]

[1]Department of Materials and Manufacturing Technology, Chalmers University of Technology, Gothenburg, Sweden
[2]Swerea IVF AB, Material Applications-Ceramics, Mölndal, Sweden
[3]GKN Aerospace Sweden AB, Trollhättan, Sweden
Email: *yiming.yao@chalmers.se

Received 6 May 2016; accepted 21 July 2016; published 25 July 2016

Abstract

This study is aiming at controlling the microstructure of plasma sprayed Al_2O_3-TiO_2 composite coatings using freeze granulated powders. As sprayed and sintered Al_2O_3 + 3wt%TiO_2 powders were air plasma sprayed with industry process parameters and compared with a commercial powder. The resulting coatings were investigated with respect to powder flowability, porosity and microstructure of the granules. The results showed that microstructure and melting fraction in the coatings could be tailored with the freeze granulation process and heat treatment conditions.

Keywords

Al_2O_3-TiO_2, Freeze Granulation, Plasma Spray, Microstructure

1. Introduction

Plasma sprayed alumina-titania coatings are well known for their excellent properties against wear, corrosion, thermal impact, and crack resistance. Therefore they have been largely applied to protect structural components and machine parts in machinery, textile, and aircraft industries [1]. Air Plasma Spray (APS) technique is a well-established industry process for applying Al_2O_3 + 3wt%TiO_2 (AT3) coatings. During the spray process, feed powder particles are injected into a plasma flame, melted and accelerated towards a substrate where they impact to form a coating [2]. The properties of the coatings depend upon the achieved microstructure, which can be controlled by both the process parameters and properties of the feedstock powder. The typical size range of powder feedstock for APS is 20 - 100 μm, and the spray parameters are usually chosen so that the powder particles are fully melted. The resulting ceramic coating has a lamellar microstructure consisting of columnar grains in splats. To achieve the required feedstock with fine particles, the powder has to be reconstituted into granules with suitable size using slurry and spray drying process. However, the conventional granule process often causes

*Corresponding author.

How to cite this paper: Yao, Y.M., Lyckfeldt, O., Tricoire, A., Lundström, D. and Klement, U. (2016) Microstructure of Plasma Sprayed Al_2O_3-3wt%TiO_2 Coating Using Freeze Granulated Powder. *Journal of Materials Science and Chemical Engineering*, **4**, 8-14. http://dx.doi.org/10.4236/msce.2016.47002

composition inhomogeneity in subsequent drying and compaction steps. An alternative technique is freeze granulation, where a powder suspension is directly sprayed into liquid nitrogen, thus the solvent is subsequently removed from the sprayed droplets (granules) by sublimation during instantaneous freezing. As a result, the encountered difficulties, e.g. granule shrinkage, strong inter-granule bonds, and the migration of small particles and additives towards the granule's surface can be efficiently prevented [3]. In the current work, AT3 granules were produced with commercial sub-micron alumina and titania powders using freeze granulation technique and compared with a commercial fused-crushed powder. This study aims to describe the influence of the feedstock powders on the microstructure and melting fraction of AT3 coatings sprayed with an industrial standard APS process.

2. Experimental

AT3 granules were fabricated using a commercial α-alumina powder (CT 3000 SG) and Anatase titania powder (Kronos 1001). The particle size distribution of the Al_2O_3 powder was d_{50} = 0.5 µm and d_{90} = 2 µm; and d_{90} < 1 µm in the TiO_2 powder. A basic AT3 powder suspension with 4 vol% PVA binder was prepared by ball milling. The slurry was then exposed to freeze granulation using ultrasonic atomization. For densification, the granules were subsequently sintered in air between 800˚C - 1600˚C for 30 min. It was found that the granule strength was poor below 1100˚C, whereas the granules sintered at 1600˚C attached firmly to each other. Therefore, the granules sintered at 1400˚C for 30 min were used for plasma spraying. The granule size is between 63 - 125 µm and the average granulation fraction is 53.3%. The granules were investigated with respect to flow performance and tap density, granule density and porosity. The granule density was calculated with excluding intrusion. Plasma spray was performed using a Sulzer Metco F4 plasma gun mounted on a 5 axis ABB IRB 2400 robot controlled by a Sulzer Metco Multicoat system. Samples were sprayed using standard parameters for production at GKN Aerospace Engine Systems. A commercial fused and crushed AT3 powder (Amperit 742, Starck) with a particle size range of 22 - 52 µm was taken as a reference. XRD analysis was performed for phase identification and phase composition. Microstructural characterization was carried out with optical microscopy, scanning electron microscopy (SEM) and energy dispersive X-ray spectroscopy (EDS).

3. Results and Discussion

Properties of Granule Powder

The characteristics of the different feed powders (fused-crushed Amperit powder, as-freeze granulated AT3 (AT3-AG)), and granulated and sintered AT3 (AT3-SG)) are summarized in **Table 1**. Amperit powder has the highest tapped density, but the flowing rate of this powder was too poor to be measured due to the angular shape of the particles. In comparison, the flow of the reconstructed granule powder is improved by the spherical morphology. With the used slip composition, the density of the as-freeze dried granules is 37% of the theoretical density (**Table 1**). The density of the granule increased to 50%, 86%, and 96% of the theoretical density (T.D.) after sintering at 1200˚C, 1400˚C and 1600˚C, respectively. **Figure 1** shows size and distribution of intrusion porosity in the granules vs. incremental pore volume. The larger volume fraction in the bimodal distribution corresponds to the space between the granules, while the smaller fraction is linked to the pores inside the granules. As can be seen, the volume of the internal pores is decreased with increased sintering temperature XRD revealed a single phase α-Al_2O_3 in both as-frozen granules and Amperit powder (**Figure 2**). After sintering at 1200˚C and 1400˚C, weak (110) and (101) reflections of rutile TiO_2 appeared. The coarse particles (22 - 52 µm) of the Amperit powder exhibit an angular and irregular morphology (**Figure 3(a)**). Most of the particles in this powder consist of 1.4 wt% Ti as a solid solute in Al_2O_3, whereas some particles with bright contrast in the backscattered electron image (BSE) in **Figure 3(a)** have a significant Ti content. In contrast, the as-freeze-granulated powder has spherical shape and a smooth surface (**Figure 3(b)**). Fine Al_2O_3 and TiO_2 particulates are distributed uniformly, and no migration of TiO_2 particulates towards the granule surface was observed (**Figure 3(c)**). With increased sintering temperature, the granule size decreased and the surface became rougher due to shrinkage and grain growth (**Figure 3(d)** and **Figure 3(e)**). TiO_2 grains (bright grains) with a size around 1 µm are homogeneously distributed in the sintered granules (**Figure 3(f)**).

Figure 2 shows XRD of the plasma sprayed coatings. The estimated phase content and porosity in the coatings are summarized in **Table 2**. The fraction of α-Al_2O_3 in the coatings indicates the amount of un-melted

Table 1. Processing and properties of feed powders.

Powder	Processing	Size (μm)	Density** (g/cm^3)	Porosity (vol%)	Flow* (s/50g)	Tapped density (g/cm^3)
Amperit	fused-crushed (Amperit)	22 - 52	fully dense	fully dense	-	1.77
AT3-SG	granulated and sintered	63 - 125	3.43	16	46.1	1.67
AT3-AG	as-freeze granulated	63 - 180	1.48	63	94.3	0.86

*Time for 50 g powder to pass through a tunnel with a 2.5 mm outlet. **Theoretical density of $Al2O_3$ + 3 wt%TiO_2 is 3.98 g/cm^3.

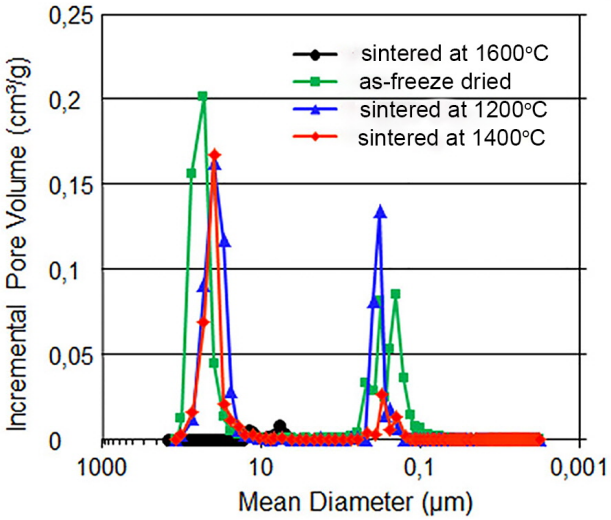

Figure 1. Size and distribution of intrusion porosity in granules vs. incremental pore volume.

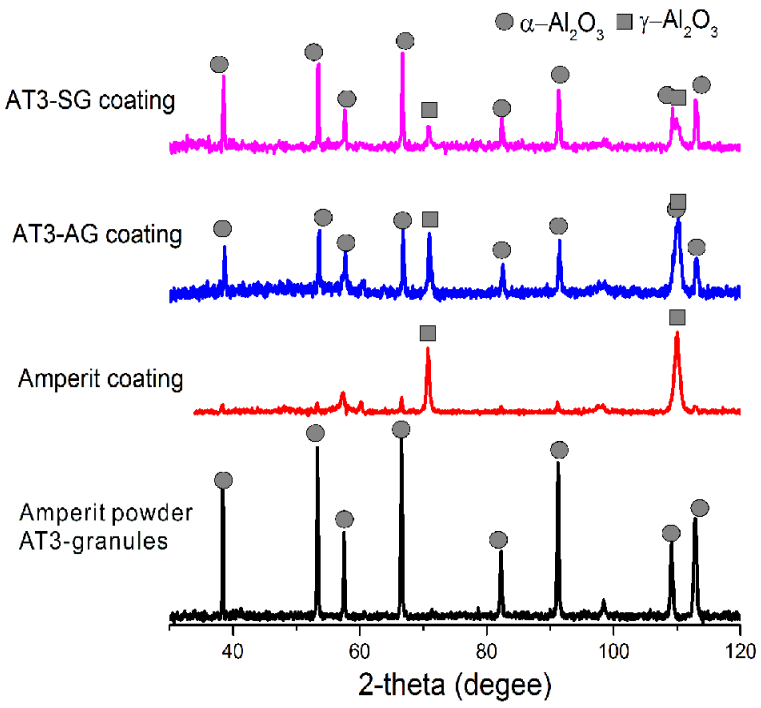

Figure 2. XRD of feedstock powder and coatings.

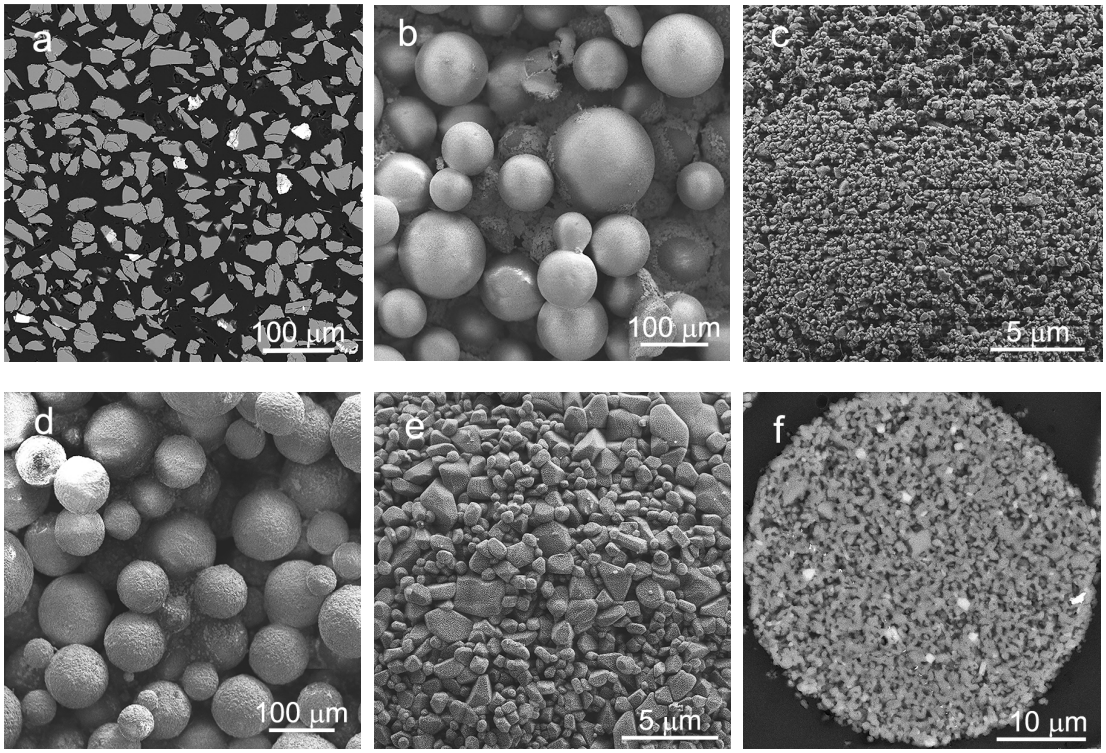

Figure 3. BSE images of feed powders, (a) cross section of Amperit powder; (b) and (c) AT3-AG granules and granule surface; (d) and (e) AT3-SG granules and granule surface; and (f) cross-section of an AT3-SG granule.

Table 2. Phase content and porosity of thermal spray coatings.

Coating	Phase content (wt%) amorphous:γ:α-	Porosity (vol%)
Amperit	29:64:7	8
AT3-AG	15:63:22	15
AT3-SG	6:22:72	16

alumina retained from the feedstock powder. The Amperit coating consists of high amounts of amorphous and metastable γ-Al_2O_3, and low amounts of α-Al_2O_3. In the AT3-AG coating, the amorphous phase is reduced and α-Al_2O_3 content is increased to 22%. In AT-3 SG coating, the α-Al_2O_3 content is increased further to 72%. The measured porosity in AT3-AG and AT3-SG coatings is double as high as in the Amperit coating. It is known that plasma sprayed alumina-titania coatings mostly consist of metastable crystalline γ-$A1_2O_3$ rather than the equilibrium α-Al_2O_3 phase, because γ-$A1_2O_3$ possesses the lowest energy barrier to nucleate from an under-cooled melt [4]. An amorphous $A1_2O_3$ is generated under super-cooling condition. The α-Al_2O_3 phase can be present in the coating as a result of incompletely melted constituents of the feedstock powders [5].

Figure 4 shows the BSE cross-sectional images of different plasma sprayed coatings. The Amperit coating shows a typical lamellar microstructure comprised of smooth splats (**Figure 4(a)**). TiO_2 rich splats (bright contrast) from coarse TiO_2 particles in the feedstock can be easily recognized. Microcracks perpendicular to the splat's surface can be observed as a result of rapid cooling (**Figure 4(b)**). The composition homogeneity is substantially improved in AT3-AG and AT3-SG coatings (**Figure 4(c)** and **Figure 4(e)**). In general, both AT3-AG and AT3-SG coatings are characterized by un-melted and partially melted structures. The AT3-AG coating consists of un-melted granule pockets embedded between fully melted splats (**Figure 4(c)**). This bimodal microstructure has been frequently observed in nanostructured Al_2O_3-TiO_2 coatings [6]. The particles in the un-melted pocket remained in submicron size (**Figure 4(d)**). From **Table 2** it can be noticed that the porosity in AT3-AG and AT3-SG coatings is nearly the same even though the AT3-AG coating was sprayed with granules of high

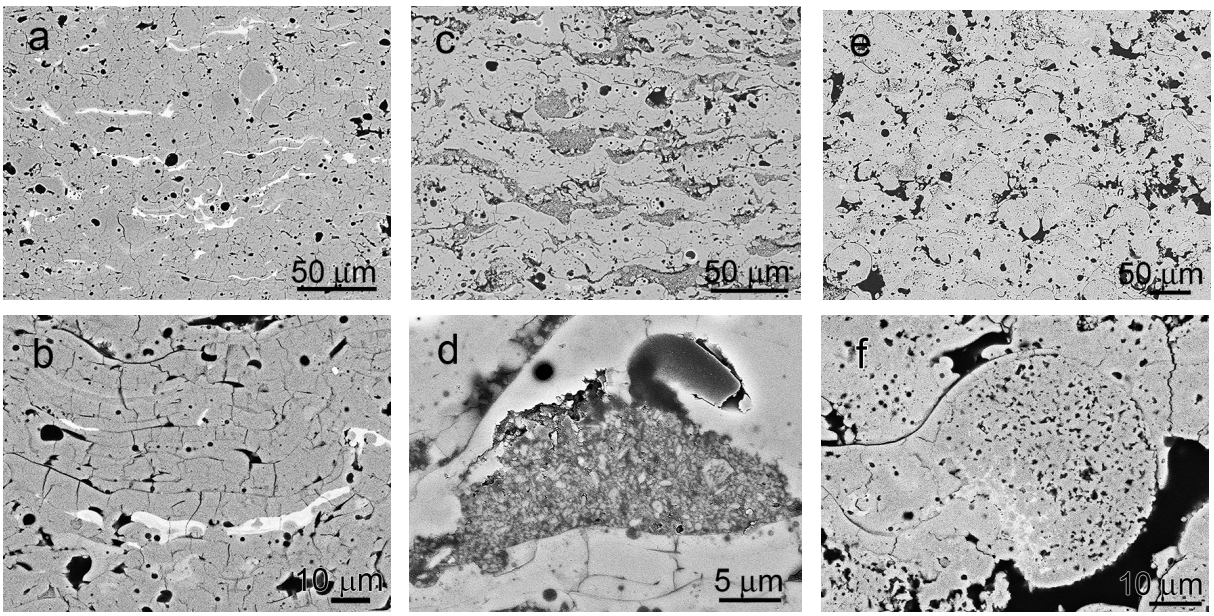

Figure 4. Microstructure of plasma spayed coatings, a) and b) Amperit coating; c) and d) AT3-SG coating; and e) and f) AT3-AG coating.

porosity. In fact, the AT3-SG coating consists of a network of un-melted sintered granule cores with diameter of 20 - 80 μm bonded with melted surface and partly melted granules (**Figure 4(e)** and **Figure 4(f)**). In the AT3-SG coating, the lamellar structure resulting from the splats is interrupted by the un-melted/partially melted granules. Moreover, the AT3-SG coating contains large pores between un-melted spherical granules in contrast to the fine pores inside un-melted regions in the AT3-AG coating. It is interesting to observe that propagation of microcracks created in γ-Al_2O_3/amorphous splats are terminated when reaching the boundaries of un-melted particle pockets and granules (**Figure 4(d)** and **Figure 4(f)**). This shows that the porous structure of the coatings can efficiently dissipate the energy of cracks originated from thermal stress and phase transformations during the spraying process.

The phase content, composition homogeneity, and lamellarity in the coating are greatly improved in the AT3 coating sprayed with the freeze-dried granules reconstructed from submicron particles. This technique provides a suitable matrix for Al_2O_3-TiO_2 composite coating materials that require a homogeneous microstructure for highly dispersed additives. For high temperature performance of the alumina-based coatings, also phase composition is important. The $\gamma - \alpha$ phase transformation occurring at 1100˚C is accompanied with a volume change of ~8%. Hence, the transformation of metastable γ-Al_2O_3 causes stress, which may results in crack formation and adhesive failure at elevated temperatures [7].

To control the un-melted fraction is critical for AT composite coatings with sensitive additives. Usually, the microstructureand un-melted fraction of the Al_2O_3-TiO_2 coatings is controlled by the critical plasma spray parameters (CPSP). The current study suggests that phase constitution and microstructure of AT3 coatings can be tailored in a wide range merely by employing freeze-dried granules with different properties. The phase transformations in the studied plasma sprayed coatings can be schematically described as depicted in **Figure 5**. The fuse-crushed α-Al_2O_3 particles of the Amperit powder were completely melted in the plasma flame to form the γ-Al_2O_3/amorphous splats and lamellar structure. In the AT3-SG coating, most of the sintered granules remained and bonded with melted/partly melted granule surfaces to form a network. In AT3-AG coating, un-melted granules were compacted to form particle pockets embedded in melted splats. The obtained microstructure is similar to that of nano-structured coatings sprayed with nano-granules [6].

The melting fraction of the particles is directly determined by the temperature the particles experience during plasma spraying. It is suggested that the particle temperature depends on both particle mass and thermal conductivity [8]. Large mass particles require higher heat to melt, thus, they are more difficult to melt than small particles, though the in-flight time in the plasma flame is longer for larger particles. The average mass of the particles is around 1, 14, and 15 mg in Amperit, AT3-AG, and AT3-SG powders, respectively (according to the data in

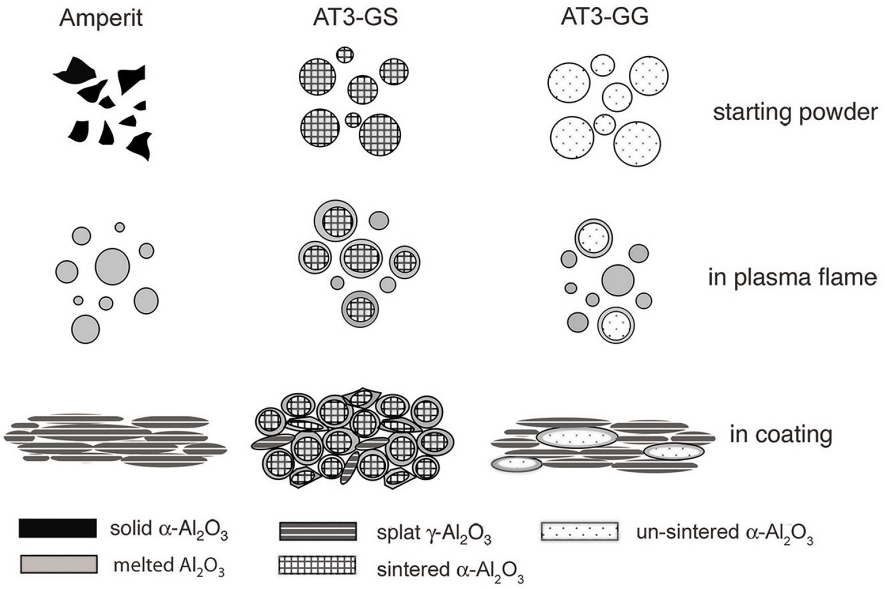

Figure 5. Representation of phase transformation and microstructural development in different AT3 feedstocks during plasma spraying.

Table 1), which is proportional to the un-melted fractions in the coatings. The temperature of granules is also affected by the porosity, which in turn influences the thermal conductivity. The granules of AT3-AG and AT3-SG with high porosity have poor thermal conductivity due the low gaseous convection of still air presenting in the internal pores. However, the higher porosity of the AT3-AG granules at similar granule mass as the AT3-SG granules was expected to provide higher un-melting fraction in the coating. It is not exclusive that some as-freeze dried granules could be crushed into small fragments during pneumatic transportation due to their intrinsic mechanical resistance. This could increase the melted fraction in the coating. Another aspect is the particle size in the granules. Small particles with higher surface area in the as-freeze dried granules are melted more easily, compared with the micron sized grains in the sintered granules (**Figure 3(d)** and **Figure 3(f)**). This can be one of the explanations for the higher melted fraction in AT3-AG than in AT3-SG coating. Therefore, granule mass, density and opening porosity of granules, strength of granule, and size of particles in granules are important aspects to influence the melting degrees in the coatings.

4. Conclusion

The freeze-dried AT3 granules consisting of submicron particles possess high followability, controllable porosity, and uniform composition distribution. Both sintered and un-sintered granules can be directly employed for APS spraying. The inhomogeneity and lamellarity of composition in the coatings are greatly improved compared to the coating sprayed with the conventional fused-crushed powder. The microstructure, phase content of γ-Al_2O_3 to α-Al_2O_3, and the melting fraction in the coating can be tailored in a wide range by adjusting the freeze granulation process and the heat treatment conditions in terms of grain size, granule size, density, pore size, and strength of the granules.

Acknowledgements

The study was financially supported by thec.

References

[1] Ctibor, P., Boháč, P., Stranyánek, M. and Čtvrtlík, R. (2006) Structure and Mechanical Properties of Plasma Sprayed Coatings of Titania and Alumina. *J. Eur. Ceram. Soc.*, **26**, 3509-3514. http://dx.doi.org/10.1016/j.jeurceramsoc.2005.12.018

[2] McPherson, R. (1989) A Review of Microstructure and Properties of Plasma Sprayed Ceramic Coatings. *Surf. Coat.*

Technol., **39-40**, 173-181. http://dx.doi.org/10.1016/0257-8972(89)90052-2

[3] Wang, Z.L., Finlay, W.H., Peppler, M.S. and Sweeney, L.G. (2006) Powder Formation by Atmospheric Spray-Freeze-Drying. *Powder Technol.*, **170**, 45-52. http://dx.doi.org/10.1016/j.powtec.2006.08.019

[4] Roychoudhary, S. and Bergman, T.L. (2004) Response of Agglomerated Multiceramic Particles to Intense Heating and Cooling for Thermal Plasma Spraying Simulation, Numerical Heat Transfer, Part A: Applications. *Journal of Computation and Methodology*, **45**, 211-233.

[5] Goberman, D., Sohn, Y.H., Shaw, L., Jordan, E. and Gell, M. (2002) Microstructure Development of Al_2O_3-13wt%TiO_2 Plasma Sprayed Coatings Derived from Nanocrystalline Powders. *Acta Mater.*, **50**, 1141-152. http://dx.doi.org/10.1016/S1359-6454(01)00414-1

[6] Kobayashi, A., Ando, Y., Kurokawa, K. and Hejwowski, T. (2011) Microstructure and Thermal Behavior of Plasma Sprayed Zirconia/Alumina Composite Coating. *J. Nanosci Nanotechnol.*, **11**, 8853-8858. http://dx.doi.org/10.1166/jnn.2011.3450

[7] Shaw, L.L., Goberman, U.D., Ren, R., Gell, M., Jiang, S., Wang, Y., Xiao, T. D. and Strutt, P.R. (2000) The Dependency of Microstructure and Properties of Nanostructured Coatings on Plasma Spray Conditions. *Surf. Coat. Technol.*, **130**, 1-8. http://dx.doi.org/10.1016/S0257-8972(00)00673-3

[8] McPherson, R. (1980) On the Formation of Thermally Sprayed Alumina Coating. *J. Mater. Sci.*, **15**, 3141-3149. http://dx.doi.org/10.1007/BF00550387